Biological Aging of CNS-Resident Cells Alters the Clinical Course and Immunopathology of Autoimmune Demyelinating Disease

Jeffrey R. Atkinson[1,2], Andrew D. Jerome[1,2], Andrew R. Sas[1,2], Ashley Munie[1,2,3], W. David Arnold[1,2], and Benjamin M. Segal[1,2]

[1]Department of Neurology, The Ohio State University Wexner Medical Center, Columbus, OH, USA.
[2]The Neuroscience Research Institute, The Ohio State University, Columbus, OH, USA.
[3]Graduate Program in Immunology, University of Michigan Medical School, Ann Arbor, MI, USA

Corresponding Author: Segal, BM
Email: Benjamin.segal@osumc.edu

Abstract

Biological aging is the strongest factor associated with the clinical phenotype of multiple sclerosis (MS). Relapsing remitting MS (RRMS) typically presents in the third or fourth decade, while the mean age of presentation of progressive MS (pMS) is 45 years old. Here we show that experimental autoimmune encephalomyelitis (EAE), induced by the adoptive transfer of encephalitogenic CD4+ Th17 cells, is more severe, and less like to remit, in middle-aged compared with young adult mice. Donor T cells and neutrophils are more abundant, while B cells are relatively sparse, in central nervous system (CNS) infiltrates of the older mice. Experiments with reciprocal bone marrow chimeras demonstrate that radio-resistant, non-hematopoietic cells play a dominant role in shaping age-related features of the neuroinflammatory response, as well as the clinical course, during EAE. Reminiscent of pMS, EAE in middle-aged adoptive transfer recipients is characterized by widespread microglial activation. Microglia from older mice express a distinctive transcriptomic profile, suggestive of enhanced chemokine synthesis and antigen presentation. Collectively, our findings suggest that drugs that suppress microglial activation, and acquisition or expression of aging-associated properties, may be beneficial in the treatment of progressive forms of inflammatory demyelinating disease.

32 ## Introduction

33 Traditionally, people with multiple sclerosis (MS) are categorized into 2 major clinical subsets based on
34 whether they experience a relapsing-remitting or progressive course. Relapsing-remitting MS (RRMS)
35 is characterized by discrete, self-limited episodes of neurological signs and symptoms that persist for
36 weeks to months, followed by a partial or full recovery. Clinical relapses are associated with the
37 appearance of acute inflammatory demyelinating lesions in central nervous system (CNS) white matter,
38 which are driven by the infiltration of lymphocytes and myeloid cells from the blood stream into the CNS
39 across leaky cerebrovascular venules (1). In contrast, progressive MS (pMS) involves an insidious,
40 gradual decline in neurological function (most often in the form of worsening paraparesis, gait
41 imbalance, and/or dementia), in the absence of focal blood-brain-barrier (BBB) breakdown or the influx
42 of peripheral immune cells. Typical pathological features of pMS include slowly expanding white matter
43 lesions, composed of a gliotic core surrounded by a rim of activated microglia, as well as widespread
44 microglia activation in the macroscopically normal appearing white matter (1, 2). Disease modifying
45 therapies (DMT) that are approved for the treatment of MS mostly target lymphocytes in the peripheral
46 immune system. While highly efficacious in RRMS, they have a modest therapeutic impact, at best, in
47 pMS. There is an unmet need for new treatments that slow, or even block, the accumulation of disability
48 in individuals with pMS. The identification of novel therapeutic targets pertinent to pMS will require a
49 deeper understanding of the pathogenic effector cells, mediators, and pathways specific to the
50 manifestation of progressive disease.

51 Biological aging is the strongest factor associated with MS clinical phenotype. RRMS typically
52 presents in the third or fourth decade, while the mean age of onset of pMS is 45 years old (3). The age
53 of onset of pMS is similar whether it occurs at clinical presentation (referred to as primary progressive
54 MS or PPMS), or follows an initial RR phase (secondary progressive MS or SPMS). Progressive MS is
55 rare before age 40, and virtually non-existent in the pediatric population (4). MS relapse rates tend to
56 decline with disease duration and chronological age (5). Collectively, these data suggest that

57 physiological changes associated with biological aging interact with the autoimmune response that
58 drives CNS damage during MS, in a manner that transforms the clinical course and underlying
59 neuropathology to a progressive pattern. Biological aging could impact the pathogenesis of MS via
60 direct effects on immune cells or CNS-resident cells. Regarding the former, aging leads to
61 immunosenescence, including a chronic, low-grade inflammatory state referred to as “inflamm-aging”.
62 Regarding the latter, aging CNS tissues may be more vulnerable to inflammatory insults and less
63 capable of initiating repair. The relative contributions of these aging-related phenomena to chronic
64 active lesions, widespread microglial activation, and accumulation of disability during pMS remains to
65 be elucidated.

66 Experimental autoimmune encephalomyelitis (EAE), the most popular animal model of MS,
67 generally presents with an acute monophasic or RR course (6). The pathological features of EAE, such
68 as multifocal BBB breakdown and CNS influx of hematogenous leukocytes, are more reminiscent of
69 RRMS than pMS. EAE is traditionally induced in young adult mice, between 8-12 weeks of age (7).
70 There is a dearth of studies examining the impact of biological aging on animal models of inflammatory
71 demyelination. Here we compare the clinical course, neuropathology, and inflammatory milieu of EAE
72 in young adult versus middle-aged mice.

73

74 Results

75 *Biological aging exacerbates the effector phase of EAE*.

76 In order to distinguish between the effect of biological aging during the T cell-priming and
77 effector stages of EAE, we employed an adoptive transfer model in which IL-23-polarized MOG_{35-55}-
78 reactive $CD4^+$ T cells from donors of different ages are injected into naïve syngeneic hosts of different
79 ages. Traditionally, EAE is induced in young adult mice, between 8 to 12 weeks of age. For the

80 middle-aged cohort, we used mice 40-44 weeks of age, based on their general developmental similarity
81 to humans at the mean age of onset for pMS (8). We found no significant differences in the clinical
82 course of EAE induced by encephalitogenic $CD4^+$ T cells derived from MOG-immunized young adult
83 versus middle-aged donors (Supplementary Figure 1). In contrast, the clinical course of EAE was
84 accelerated and exacerbated in middle-aged, compared with young adult, recipients that had been
85 injected with the same pool of encephalitogenic $CD4^+$ T cells (Fig. 1). Middle-aged recipients developed
86 neurological deficits earlier, had higher peak scores, and more cumulative neurological disability (Fig. 1
87 A-C). Middle-aged recipients exhibited increased weight loss, and a significant proportion succumbed
88 to disease (58%), while all of the young recipients survived (Fig.1 D, E). Moreover, approximately 80%
89 of young adult recipients underwent clinical remission, compared with approximately 40% of their
90 middle-aged counterparts (Fig. 1 F). This divergence in clinical courses between the 2 groups was
91 reflected in pathological findings. Immunohistochemical analysis of spinal cord sections revealed more
92 extensive demyelination, associated with parenchymal infiltration by $CD45^{hi}$ hematogenous leukocytes,
93 in the middle-aged cohort (Fig. 2). Electrophysiological studies were performed to assess the functional
94 integrity of the spinal cord. Motor-evoked responses following cervical spinal cord stimulation showed
95 slower delayed responses in all mice at peak and chronic stages of EAE compared with baseline,
96 indicative of demyelination in the corticospinal tracts (Fig. 3B). The delay in nerve signal propagation
97 was significantly longer in middle-aged hosts (Fig. 3C), consistent with the enhanced myelin damage
98 that was revealed by immunohistochemistry. In addition, middle-aged mice exhibited a greater
99 reduction in motor-evoked potential amplitudes compared with young adult mice, signifying increased
100 axonal dysfunction and/or loss (Fig. 3B, D). Motor unit number estimation (MUNE) is calculated by
101 dividing the maximum compound muscle action potential amplitude, obtained with sciatic nerve
102 stimulation, by the average single motor unit potential. MUNE, which reflects the number of motor units
103 innervating single muscles, was also lower in the sciatic innervated hindlimb muscles of middle-aged
104 hosts (Fig. 3E), consistent with a greater loss or dysfunction of motor neurons in the lumbar spinal cord.

105 *Encephalitogenic T cells and neutrophils are expanded, while B cells are retracted, in CNS infiltrates of*
106 *middle-aged mice with EAE*.

107 The exacerbated clinical course of EAE in older mice could be secondary to a more virulent
108 neuroimmune response, increased susceptibility of CNS resident cells/myelin to immune-mediated
109 damage, or a combination of these mechanisms. To investigate the former possibility, we compared the
110 cellular composition of neuroinflammatory infiltrates between middle-aged and young adult mice on day
111 10 post-T cell transfer. There were significantly higher frequencies of $CD4^+$ T cells and neutrophils, and
112 a lower frequency of B cells, among $CD45^+$ cells isolated from the spinal cords of the middle-aged
113 recipients (Fig. 4A-C). There were no differences between groups in the frequencies of macrophage/
114 monocytes or monocyte-derived dendritic cells (Supplementary Figure 2). For our experiments, we
115 routinely obtain MOG_{35-55}-primed $CD4^+$ T cells from $CD45.1^+$ congenic donors, in order to distinguished
116 the transferred encephalitogenic T cells from $CD45.2^+$ bystander host T cells. We found that $CD45.1^+$
117 $CD4^+$ T cells were disproportionately expanded in the CNS of middle-aged recipients (Fig. 4B). A broad
118 panel of pro-inflammatory and chemotactic factors were up-regulated in spinal cord lysates of all mice
119 with EAE, but were consistently elevated to higher levels in older mice. These factors include the
120 chemokines CCL5, CXCL9 and CXCL10, which have been shown to target encephalitogenic T cells (9,
121 10), and CXCL1 and CXCL2, the major chemoattractants of mature neutrophils (11, 12) (Fig. 5).
122 Neutrophil-mobilizing factors GM-CSF and G-CSF were also expressed at higher levels in older mice.
123

124 *GM-CSF promotes the early, but not late, stage of exacerbated EAE in aged mice.*

125 We have previously shown that GM-CSF receptor (GM-CSFR)-deficient mice are relatively
126 resistant to adoptively transferred EAE (13). They experience a milder course than WT counterparts,
127 with an increased rate of remission. In addition, GM-CSFR deficiency is associated with a lower percent
128 of $CD4^+$ donor T cells and neutrophils, and a higher percent of B cells, in CNS infiltrates, which is the
129 mirror image of the pattern that we observed in middle-age, wild-type mice with EAE. Collectively, these
130 observations suggest that the exacerbated form of EAE that occurs in middle-aged wildtype mice is

131 GM-CSF-driven. Indeed, the absolute number of GM-CSF-expressing donor $CD4^+$ T cells in CNS
132 infiltrates, the level of intracellular GM-CSF in CNS donor T cells, and the level of GM-CSF protein in
133 CNS lysates, were higher in the older versus younger mice with EAE (Fig. 5, Fig.6A, B). Furthermore,
134 single-cell RNA sequencing revealed heightened expression of transcripts encoding GM-CSF, as well
135 as IL-17 and other pro-inflammatory factors, in $CD4^+$ T cells isolated from the CNS of middle-aged mice
136 on day 6 post-transfer, when compared with their younger counterparts (data not shown). Treatment of
137 middle-aged hosts with a neutralizing antibody against GM-CSF, beginning from the day of transfer
138 onward, delayed clinical onset and ameliorated the early clinical course (Fig. 6C, D). However, mean
139 peak scores, cumulative chronic disability, and mortality rates were similar between the anti-GM-CSF
140 and control antibody treatment groups (Fig. 6 C, E, and data not shown). Postponing the initiation of
141 anti-GM-CSF treatment to the time of peak disease had no therapeutic impact (data not shown). Based
142 on these data, we concluded that GM-CSF promotes aggressive EAE in older recipients in the early
143 phase of disease, but becomes dispensable as the disease progresses towards a more chronic phase.
144
145 *Radio-resistant, non-hematopoietic cells shape the neuroinflammatory infiltrate and drive exacerbated*
146 *EAE in middle-aged mice.*
147 Next, we sought to determine whether the increased susceptibility of older mice to EAE is
148 secondary to the biological aging of radio-sensitive, hematopoietic cells (that are recruited from the
149 circulation to the CNS) and/or radio-resistant, non-hematopoietic cells (including CNS-resident cells).
150 To that end, we constructed reciprocal bone marrow (BM) chimeric mice with young or middle-aged BM
151 cell donors and/or irradiated hosts (Fig. 7A). Middle-aged → middle-aged and young adult → young
152 adult chimeras served as controls. EAE was induced in all immune reconstituted chimeric mice via the
153 adoptive transfer of the same pool of MOG_{35-55} encephalitogenic $CD4^+$ T cells. Irrespective of the age of
154 the BM cell donors, BM cell hosts that were middle-aged experienced a severe clinical course of EAE,
155 with high mortality rates, while young adult BM cell hosts experienced a milder course with relatively
156 low mortality rates (Fig. 7 B, C). Furthermore, the cellular composition of neuroinflammatory infiltrates in

157 chimeras correlated with the age of the BM cell host, but not the donor, mouse. Middle-aged BM cell
158 hosts contained higher frequencies of $CD4^+$ T cells in EAE lesions compared with chimeras that were
159 constructed using young adult hosts, mimicking the results we obtained with non-chimeric mice (Fig.
160 7D, left panel). Furthermore, the frequency of B cells tended to be lower, while that of neutrophils
161 tended to be higher, in CNS infiltrates of middle-aged hosts, though not reaching statistical significance
162 (Fig. 7D, middle and right panels). Hence, the age of radio-resistant, non-hematopoietic cells is a
163 dominant factor in determining the phenotype and severity of EAE.
164
165 *Aged microglia exhibit distinct transcriptomes and phenotypes during homeostasis, as well as EAE.*
166 Our finding that radio-resistant cells influence the make-up of neuroinflammatory infiltrates
167 directed our attention towards the role of microglia. In addition to their potential to serve as antigen-
168 presenting cells, microglia produce chemotactic and pro-inflammatory molecules that could orchestrate
169 the recruitment, positioning, and polarization of leukocyte subsets in EAE lesions. A growing body of
170 data indicates that microglia become spontaneously activated and acquire pro-inflammatory signatures
171 with age (14, 15). In support of these published studies, we found that a significant percent of microglia
172 in naïve middle-aged, but not young adult, mice exhibit enhanced expression of the cell surface marker
173 CD11c (Fig. 8). Bulk RNA sequencing studies showed that the aged microglia in unmanipulated mice
174 express elevated levels of activation markers compared with their younger counterparts (data not
175 shown). Furthermore, a number of genes that were disproportionately up-regulated in the middle-aged
176 microglia (such as *Ccl4*, C*xcl10*, and S*pp1*) overlapped with previously published transcriptomes of
177 aging microglial subsets (data not shown) (14).
178 Next, we performed single-cell RNA sequencing of CNS $CD45^+$ mononuclear cells isolated from
179 young adult and middle-aged mice during peak EAE. The microglial cells fell into 2 clusters. Cluster 1
180 microglia from middle-aged mice express high levels of genes encoding chemotactic factors (including
181 *Ccl4, Ccl6, Cxcl2, Cxcl9,* and *Cxcl10*) and low levels of genes associated with homeostasis (including
182 *Fcrls*, *Tmem119*, *P2ry12*, and *Cx3cr1*) compared with their counterparts from young mice (data not

183 shown). Cluster 2 microglia from middle-aged mice are relatively enriched in transcripts associated with
184 antigen processing and presentation (including *H2-Aa, H2-Ab1, H2-D1, H-2-Eb1, H2K1, H-2Q7, B2m,*
185 *and Cd74*), and proteasome assembly and function (*Psmb4, Psmb8, Psmb9, Psmb10, Psme1,*
186 *Psme2*), as well as transcripts that encode pro-inflammatory molecules (*TNF*, *IL1a*, *IL1b*, *IL18*). In
187 contrast, they are relatively deficient in transcripts associated with homeostasis (*Tmem119*, *Fcrls,*
188 *Cx3cr1, and P2ry12*) and heat shock protein responses *(Dnaja1, Dnajb1, Hspa1a*, *Hspa1b*, *Hspa5*,
189 *Hsp90aa1*, *Hsp90ab1*) (data not shown). Middle aged microglia in both clusters expressed relatively
190 high levels of interferon responses genes (including *Gbp2*, *Ifitm3*, I*fi27l2a*, *Isg15)*, as well as genes
191 expressed at high levels in microglia located at the rims of slow expanding lesions in people with pMS
192 (*C1qa*, *C1qb*, *C1qc*, *Cstb*, *Fth1*, *Ftl1*, and a panel of ribosomal proteins).
193

194 ## Discussion

195 Progressive MS typically presents during middle age, whether or not it is preceded by a RR course. It
196 rarely, if ever, occurs in the pediatric MS population (4). Progressive MS has distinctive pathological
197 features that are not characteristic of RRMS in younger individuals, including widespread microglial
198 activation (1). These observations indicate that biological aging has a profound influence on the
199 evolution and manifestation of autoimmune neuroinflammation, but the underlying mechanisms are
200 poorly understood. Here we show that EAE, induced by the transfer of a common pool of IL-23-
201 polarized, MOG-reactive $CD4^+$ T cells, is more severe, and less likely to remit, in middle-aged
202 compared with young adult recipients. We employed an adoptive transfer model in order to distinguish
203 between age-dependent environmental factors in the recipient mouse, as opposed to intrinsic
204 properties of encephalitogenic T cells, that might contribute to the differences in EAE phenotype
205 between the cohorts. The heightened, refractory disability exhibited by older adoptive transfer recipients
206 may reflect an increased vulnerability of aged oligodendrocytes, myelin and/or axons to immune-
207 mediated damage. However, our data indicate that aging has an impact on neuroinflammation itself,

208 since the cellular composition of $CD45^+$ cells in the CNS at peak EAE differs markedly between young
209 adult and middle-aged recipients. Donor T cells and neutrophils were consistently more abundant, while
210 B cells were relatively sparse, in the CNS of older mice. Our experiments with reciprocal bone marrow
211 chimeric mice indicate that radio-resistant, non-hematopoietic cells play a dominant role in shaping
212 age-related features of the neuroinflammatory response, as well as the clinical course, during EAE.
213 Among radio-resistant host cells, glia are strong candidates for regulators of CNS autoimmunity.

214 We found that murine microglia spontaneously upregulate CD11c as they age. This is
215 consistent with previous reports that aging microglia exhibit morphological, phenotypic, and
216 transcriptomic changes indicative of a predisposition towards an activated or pro-inflammatory state
217 (16-18). Our working hypothesis is that the increased susceptibility of middle-aged mice to
218 encephalitogenic T cell accumulation, white matter damage, and exacerbated clinical EAE, is driven, at
219 least in part, by aging microglia. Indeed, enhanced microglial reactivity in the aging monkey brain
220 correlates with an increase in perivascular T cell infiltrates in the white matter parenchyma, as well as
221 cognitive impairment (19). Interestingly, genes we found to be highly expressed by microglia from
222 middle aged adoptive transfer recipients are also expressed at high levels by microglia located in the
223 rims of chronic active lesions during pMS, including genes involved in expression of the MHC-II protein
224 complex, ferritin complex, and complement cascade (data not shown).

225 The mechanisms underlying age-related changes in microglia are likely multifold. Neuronal
226 maintenance of microglial homeostasis via CX3CL1/CX3CR1 and CD200/CD200R interactions wanes
227 with aging (20-22). In addition, microglia can be stimulated by CNS-penetrant, pro-inflammatory factors,
228 such as IL-6, CCL11, and IL-1β, that are systemically released by peripheral immune cells in the
229 context of “inflamm-aging”, and/or by microbiome-derived molecules, such as LPS, that rise in the
230 bloodstream consequent to age-related increases in gastrointestinal permeability (17, 18, 23-25).
231 Microbial metabolites, which are altered during dysbiosis, also modulate microglial function in an age-
232 dependent fashion. In young adults, gut microbiome-derived tryptophan metabolites and short chain

233 fatty acids (SCFA) cross the blood-brain-barrier and constitutively suppress microglia, thereby reducing
234 the risk of neuroinflammation (26, 27). Dietary supplementation with the SCFA propionic acid is
235 associated with less inflammatory activity, disability progression, and brain atrophy in MS (28).
236 However, production of SCFAs and tryptophan metabolites by gut bacteria declines with aging (29),
237 thereby removing another check on microglial activation.

238 Single-cell RNA sequencing of $CD45^+$ leukocytes, harvested from the CNS at peak disease,
239 revealed 2 clusters of EAE-associated microglia, both of which exhibit dynamic, age-dependent
240 transcriptomic signatures (data not shown). By comparison to their counterparts harvested from young
241 adult adoptive transfer recipients, cluster 2 microglia from middle-aged recipients are highly enriched in
242 transcripts that encode molecules engaged in the presentation of antigen to T cells. This finding led us
243 to hypothesize that more efficient antigen presentation by cluster 2 microglia might boost the
244 proliferation of donor T cells, resulting in higher T cell frequencies within the CNS infiltrates of middle-
245 aged mice. However, contrary to that hypothesis, we found comparable frequencies of $Ki67^+$ donor T
246 cells among $CD45^+$ CNS mononuclear cells isolated from young adult or middle-aged mice at peak
247 EAE (data not shown). Furthermore, $CD45^{int}CD11b^+$ microglia, purified from young adult or middle-
248 aged mice at peak EAE, stimulated the proliferation of 2D2 cells (T cell receptor transgenic $CD4^+$ cells
249 specific for MOG peptide) to a similar degree (data not shown). To further investigate this issue, in
250 future experiments we will compare the proliferation of donor T cells, and the antigen-presenting/T cell-
251 polarizing capacity of sharply-defined microglial subsets, in young adult versus middle-aged hosts at
252 multiple time-points. Interestingly, some of the transcripts upregulated in cluster 2 microglia from
253 middle-aged mice are involved in the assembly and function of proteasomes and processing of MHC
254 Class I restricted peptides. Although our model of EAE is $CD4^+$ T cell-driven, $CD8^+$ T cells are more
255 prevalent than $CD4^+$ T cells in human MS lesions, including in the chronic active lesions that are typical
256 of pMS (30-32). The emergence of microglia particularly well-equipped to activate $CD8^+$ T cells might
257 be relevant to the pathogenesis of pMS.

258 In middle-aged hosts, cluster 1 microglia are enriched in transcripts that encode a range of
259 chemokines including CXCL2 and CXCL10. We and others previously showed that neutrophil migration
260 to the CNS during EAE is dependent on CXCR2-binding chemokines (such as CXCL1, CXCL2)(11, 12,
261 33, 34), while $CD4^+$ T cell migration is dependent on CXCR3-binding chemokines (such as CXCL9,
262 CXCL10 and CXCL11) (9). Elevated production of CXCL2 and CXCL10 by aged cluster 1 microglia
263 might trigger preferential accumulation of donor T cells and neutrophils locally, and thereby underlie the
264 relative enrichment of those subpopulations in the CNS of middle-aged hosts. The translational
265 significance of this finding is underscored by the observations that pMS patients have a relatively high
266 percentage of circulating $CXCR3^+$ lymphocytes(35), and $CXCR3^+$ lymphocytes preferentially
267 accumulate in MS lesions (36). Furthermore, CXCL9 and CXCL10 are up-regulated in pMS brains[33],
268 and expression of CXCR3 on circulating $CD8^+$ T cells correlates with MS lesion volume (37). There is
269 also evidence that neutrophil-related factors and chemokines are dysregulated in pMS and correlate
270 with clinical, as well as radiological, measures of CNS tissue damage (25).

271 In addition to sculpting the neuroinflammatory response via antigen presentation and chemokine
272 production, aging microglia could modulate EAE by releasing soluble factors that directly damage
273 oligodendrocytes and/or axons, such as reactive oxygen and nitrogen species, enzymes and TNF
274 family members (38, 39), and/or that drive the polarization of neurotoxic astrocytes, such as IL-1α and
275 C1q (27, 40). Conversely, we found that aging microglia in cluster 2 downregulate expression of
276 transcripts encoding heat shock proteins 90 and 70, which have been implicated in neuroprotection and
277 the suppression of neurotoxic astrocytes, respectively (41, 42). Increased susceptibility of
278 oligodendrocytes and neurons/axons to immune-mediated insults, combined with impairment of
279 microglial phagocytosis, might escalate CNS deposition of danger-associated molecular patterns
280 (DAMPs) and cellular debris in middle-aged hosts. DAMPs and cellular debris incite the activation of
281 microglia and infiltrating leukocytes, which could fuel a self-amplifying cycle of tissue destruction.
282 Although the adoptive transfer model of EAE in middle-aged mice lacks a number of salient

283 pathological features of pMS (i.e. slowly expanding, chronic active lesions and cortical lesions), it may
284 be useful for investigating how biological aging alters inflammatory demyelinating disease in other ways
285 that simulate progressive MS (i.e. diffuse microglial activation and a non-remitting clinical course), and
286 for testing the efficacy of senolytic drugs, microglial suppressors, or other novel therapeutic
287 interventions potentially beneficial in the pMS subpopulation.

288

289 Methods

290

291 *Mice.*

292 CD45.1 congenic and wild-type C57BL/6 mice were obtained from Charles River Laboratories or the
293 National Cancer Institute. Mice were housed in micro-isolator cages under specific pathogen-free
294 conditions at the Ohio State University. Both male and female mice were used in experiments.

295

296 *Induction and assessment of EAE*.

297 8-12 week old mice were immunized subcutaneously with an emulsion consisting of 100 μg of MOG_{35-55}
298 peptide (MEVGWYRSP-FSRVVHLYRNGK; Biosynthesis) emulsified in Complete Freund's Adjuvant
299 (CFA; Difco), at four sites over the flanks. Inguinal, axial, and brachial lymph nodes and spleens were
300 harvested from donor mice 10-14 days post-immunization and passed through a 70 μm strainer (Fisher
301 Scientific) to obtain a single-cell suspension. The cells were cultured for 96 hours with MOG_{35-55} peptide
302 (50 μg/mL) and Th17-polarizing factors as follows: recombinant murine (rm)IL-23 (8 ng/ml; R&D
303 Systems), rmIL-1α (10 ng/ml; Peprotech) and anti–IFNγ (10 μg/ml; clone XMG1.2, Bio X Cell). After 96
304 hours, the cells were harvested, washed and resuspended in fresh media. $CD4^+$ T cells were purified
305 via positive-selection, magnetic-activated cell sorting (MACS) using L3T4 magnetic microbeads
306 (Miltenyi Biotec) per the manufacturer's protocol. $CD4^+$ T cells (90-98% purity) were transferred via

307 intraperitoneal (i.p.) injection to naïve C57BL/6 recipients. Recipient mice were weighed and observed
308 daily for clinical disability and rated using a 5-point scale as described previously. Briefly, 0.5, partial tail
309 paralysis; 1, full tail paralysis; 1.5, hindlimb weakness demonstrated by ability to correct from a prone
310 position in <1s; 2, hindlimb weakness demonstrated by ability to correct from a prone position in >1s;
311 2.5, hindlimb weakness demonstrated by severe gait abnormality; 3, partial hindlimb paralysis
312 demonstrated by the inability to elevate hindquarters; 3.5 complete paralysis in one hindlimb; 4,
313 complete hindlimb paralysis; 4.5, moribund; and 5, dead.

314

315 *CNS mononuclear cell and homogenate collection.*

316 Mice were anesthetized with isoflurane and perfused with 1x PBS. The brain was removed from the
317 skull, and the spinal cord was flushed through the spinal canal with PBS. Combined brain and spinal
318 cord tissues were homogenized with an 18-gauge needle in a protease inhibitor solution created using
319 protease inhibitor cocktail tablets (Roche) per the manufacturer's protocol, centrifuged at 800 g for 5
320 minutes, and the supernatant was collected and stored at -80°C. Tissue pellet was resuspended in a
321 solution of HBSS with 1 mg/ml collagenase A (Roche) and 1 mg/ml DNase I (Sigma-Aldrich) and
322 incubated at 37°C for 20 minutes. Mononuclear cells were separated from myelin via centrifugation in a
323 27% Percoll solution (GE Healthcare).

324

325 *Fluorescent immunohistochemistry.*

326 Spinal cords were harvested from mice perfused with 1x PBS and 4% paraformaldehyde (PFA). Tissue
327 were post-fixed with 4% PFA for 24 hours, washed with 1x PBS, decalcified with 0.5 M EDTA for 4-6
328 days, and cryopreserved with 30% sucrose solution at 4°C. Tissue was embedded in OCT for
329 cryosectioning and stored at -80°C. Sections were blocked with 5% normal goat serum (Sigma-Aldrich),
330 washed with 0.1% Triton-X 100 (Fisher Scientific) in 1x PBS (PBS-T), and stained with rat anti-mouse

331 CD45 (clone IBL-5/25; EMD Millipore) for 48 hours at 4°C. Following washing with PBS-T, sections
332 were stained with Alexa Fluor 647 goat anti-rat IgG (Invitrogen) for 2 hours. Sections were then stained
333 with FluoroMyelin Red Fluorescent Myelin Stain (Invitrogen) per the manufacturer's protocol. ProLong
334 Gold antifade reagent with DAPI (Invitrogen) was applied immediately prior to applying the coverslip.
335 Images were acquired using an Olympus IX83 inverted fluorescent microscope with cellSens
336 Dimension software (Olympus).

337

338 *Electrophysiology.*

339 Electrophysiological recordings were performed using a clinical electrodiagnostic system (Cadwell).
340 During recordings mice were anesthetized using ketamine/xylazine anesthesia. A petroleum-based eye
341 lubricant (Dechra) was applied to prevent corneal irritation and dryness. A thermostatically-controlled,
342 far infrared heating pad was used to maintain body temperature (Kent Scientific). Hair from the right
343 hindlimb was removed with clippers (Remington, model VPG 6530) to allow for adequate electrode-skin
344 contact. During anesthetized recordings, mice were placed in the prone position, and bilateral hindlimbs
345 were extended and affixed to the heating pad with Transpore medical tape (3M). Compound muscle
346 action potential (CMAP) and single motor unit potential (SMUP) amplitudes were recorded from the
347 right gastrocnemius muscle similar to our prior studies in aged mice(43, 44). Briefly, a pair of recording
348 ring electrodes (Alpine Biomed) were placed at the proximal gastrocnemius (G1) and at the mid-tarsal
349 region of the hind paw (G2). The skin underneath the ring electrodes was coated with electrode gel
350 (Parker Laboratories) to reduce skin impedance. A disposable surface disc electrode was placed on
351 the surface of the skin of the tail (Natus Neurology) as the common reference electrode (G0). Two 28-
352 gauge monopolar electrodes (Natus Neurology) were inserted subcutaneously at the proximal right
353 thigh and used as the cathode and anode to stimulate the sciatic nerve. A constant current stimulator
354 was used to deliver pulses (0-10 mA current, 0.1 ms duration). Supramaximal stimulation was delivered
355 to record the maximum CMAP amplitude. Then the stimulus was reduced, and a gradually increasing

356 stimulus was used to elicit a total of 10 all-or-none CMAP increments. The 10 incremental responses
357 were averaged to determine the average SMUP amplitude which was used to calculate motor unit
358 number estimation (MUNE = maximum CMAP / Average SMUP). To determine CMAP response
359 following spinal cord conduction, the stimulating electrodes were placed subcutaneously at the base of
360 the skull on each side of the spinal column. The spinal cord was stimulated using a constant current
361 stimulator (0-40 mA, 0.2 ms) to elicit the maximum cervical motor evoked potential (MEP) amplitude.
362 During all recordings, high and low frequency filter settings were set at 10 kHz and 10 Hz, respectively.
363 Peak-to-peak amplitudes were used for all analyses.

364

365 *Flow cytometry*

366 For surface staining, cells were resuspended in 1x PBS with 2% fetal bovine serum (FBS), fixable
367 viability dye (eFluor506, eBioscience), and anti-CD16/32 (clone 2.4G2, hybridoma, ATCC). Cells were
368 then labeled with fluorescently labeled monoclonal antibodies specific for individual markers. For
369 intracellular cytokine staining, cells were stimulated with PMA (50 ng/ml), ionomycin (2 µg/ml), and BFA
370 (5 µg/ml) for 4–6 hours. Cells were then fixed and permeabilized with the Fixation/Permeablization Kit
371 (BD Biosciences) according to the manufacturer's protocols and incubated with fluorescently labeled
372 monoclonal antibodies. Data were acquired using a FACSMelody flow cytometer (BD Biosciences) and
373 analyzed with FlowJo software (Tree Star).

374

375 *Antibodies*

376 The following antibodies were obtained from eBiosciences: CD11b (M1/70)- APC-eFluor 780, CD11c
377 (N418)- PerCP-Cyanine5.5, CD45.1 (A20)- FITC and PE, CD45R/B220 (RA3-6B2)- PE, and Ki-67
378 (SolA15)- PE-Cyanine7. The following antibodies were obtained from Invitrogen: CD45 (30-F11)-
379 eFluor 450 and GM-CSF (MP1-22E9)- FITC. The following antibodies were obtained from BD

380 Pharmingen: Ly6G (1A8)- PE-Cy7. The following antibodies were obtained from BioLegend: CD4
381 (RM4-5)- APC. For *in vivo* GM-CSF blocking experiments, 500 µg of anti-mouse GM-CSF (MP1-22E9)
382 or rat IgG2a isotype control (2A3) (Bio X Cell) were administered via i.p. injection.

383

384 *Multiplex cytokine assay*

385 Cytokine levels were measured in spinal cord homogenates by Luminex multiplex bead-based analysis
386 (MILLIPLEX MAP Mouse Cytokine/Chemokine Magnetic Bead Panel; Millipore) using the Bio-Plex 200
387 system (Bio-Rad Laboratories) according to the manufacturer's protocols.

388

389 *Generation of bone marrow chimeras*

390 Femur, tibia, and humorous bones were harvested from donor mice. Marrow was flushed from the
391 bone, passed through a 70 µm mesh filter to generate a single-cell suspension, and red blood cells
392 were lysed by a brief incubation in ACK lysis buffer (Quality Biological). Hosts were lethally irradiated
393 with 2 doses of 6.5 Gy and reconstituted by tail vein injection of 2-4 x 10^6 donor bone marrow cells.
394 Recipient mice were allowed to reconstitute for 6 weeks prior to use.

395

396 *Schematic design*

397 All figure schematics were created using BioRender software.

398

399 *Single-cell RNA-seq analysis*

400 <u>Sequence mapping and preprocessing:</u> Mononuclear cells isolated from 4 spinal cords per group and
401 processed following the 10X Genomics Chromium Single Cell RNA v3 protocol. Libraries were

402 sequenced on an Illumina Novaseq instrument and counted with CellRanger v3.1.0 using mm10
403 reference genome GENCODE vM23/Ensembl 98). Data processing and visualizations of the scRNA-
404 seq data were performed using the Seurat package (v.4.0.4) in R (4.1.0). For the initial quality control
405 filtering, we removed individual cells that detected less than 200 genes or more than 25,000 reads, and
406 genes that were detected in less than three cells. We filtered outlier cells that were outside the range of
407 5x median absolute deviation of the in that cell due to sequencing depth using scater. We also only
408 retained cells with less than 10% mitochondrial reads and less than 50% ribosomal reads. Data were
409 scaled to 10,000 transcripts per cell, and transformed to log space using Seurat's LogNormalize
410 method. The top 2,000 highly variable genes in the each sample were computed based on dispersion
411 and mean.

412 Data integration and cell clustering To correct the batch effect, anchor genes were identified from all
413 samples using the *FindIntegrationAnchors* function in Seurat on the first 20 dimensions, and integrated
414 using Seurat *IntegrateData*() function. Principal component analysis (PCA) was performed on the
415 variable genes. The top 20 PCs were used to build a k-nearest-neighbors cell-cell graph with k = 30
416 neighbors. Cell clusters were identified by the use of the Louvain graph-clustering algorithm with a
417 resolution set to 0.4. For each cell cluster, we assigned the cell-type labels using small sets of known
418 marker genes and cluster-specific genes. The dataset was projected onto the two-dimensional space
419 using uniform manifold approximation and projection (UMAP) dimensionality reduction with default
420 parameters.

421 DEG analysis and enrichment test: We identified cluster-specific genes for the clusters using the
422 *FindAllMarkers* function, comparing the gene expression levels in a given cluster with the rest of the
423 cells. The significance of difference was determined using a Wilcoxon Rank Sum test with Bonferroni
424 correction. Differentially expressed genes (DEG) are determined by setting threshold of adjusted p-
425 value of < 0.05 and absolute log2-foldchange > 0.25. We computationally selected individual cell types
426 for between-group differential gene expression analysis. Note that the batch corrected integration data

427 was only used for cell clustering and dimensional reduction, and the differential gene expression
428 analysis was performed using the normalized RNA assay slot in Seurat. Pathway enrichment analysis
429 was performed using Enrichr using libraries including GO_2018 and KEGG_2019_MOUSE. We also
430 used clusterProfiler's universal enrichment analyzer to analyze our manually selected GO pathways
431 and overlapping DEGs with public datasets. To visualize DEGs, volcano plots were generated using
432 EnhancedVolcano. Heatmaps were generated using ComplexHeatmap on z-score transformed
433 normalized gene expression values.

434 Individual FASTQ files were trimmed for adapter sequences and filtered using fastp v0.20.0. Mouse
435 reference genome GRCm38.p6 and gene annotation described by Gene Transfer Format (GTF) were
436 downloaded from Ensembl release 99 (January 2020). Reads alignment was performed against the
437 reference genome using HISAT2 v2.1.0. Gene expression values for genes were quantified using the
438 featureCounts tool of the Subread package v1.5.0-p2 in unstranded mode. Genes detected in less than
439 10 total counts in at least 3 samples were removed from downstream analysis. The fold-change was
440 calculated using CPM-normalized values using EdgeR.

441

442 *Statistical Analysis of clinical, proteomics and flow cytometric data*

443 Statistical analysis was performed in GraphPad Prism using paired or unpaired 2-tailed Student's t test,
444 or 1-way or 2-way ANOVA with correction for multiple comparisons, as indicated in the legends.
445 Disease curves were compared by unpaired t tests with a Welch correction at individual days where
446 indicated. Comparison for incidence, survival, and remission curves were performed using a Log-rank
447 test. Outliers were identified by ROUT analysis and removed as necessary. A p value less than 0.05 (*)
448 was considered significant; **p <0.01, ***p <0.001, and ****p <0.0001.

449

450 *Study approval*

All animal experiments were performed in accordance with an IACUC-approved protocol at The Ohio State University.

Acknowledgements

This work was supported by National Institute of Neurological Disorders and Stroke grant R01 NS105385 (to BMS). BMS is the Stanley and Joan D. Ross Professor of Neuromodulation.

457 # References

458 1. Lassmann H. Pathogenic Mechanisms Associated With Different Clinical Courses of Multiple
459 Sclerosis. *Front Immunol.* 2018;9:3116.
460 2. Frischer JM, Weigand SD, Guo Y, Kale N, Parisi JE, Pirko I, et al. Clinical and pathological
461 insights into the dynamic nature of the white matter multiple sclerosis plaque. *Ann Neurol.*
462 2015;78(5):710-21.
463 3. Tutuncu M, Tang J, Zeid NA, Kale N, Crusan DJ, Atkinson EJ, et al. Onset of progressive phase
464 is an age-dependent clinical milestone in multiple sclerosis. *Mult Scler.* 2013;19(2):188-98.
465 4. Harding KE, Liang K, Cossburn MD, Ingram G, Hirst CL, Pickersgill TP, et al. Long-term
466 outcome of paediatric-onset multiple sclerosis: a population-based study. *J Neurol Neurosurg*
467 *Psychiatry.* 2013;84(2):141-7.
468 5. Tremlett H, Zhao Y, Joseph J, Devonshire V, and Neurologists UC. Relapses in multiple
469 sclerosis are age- and time-dependent. *J Neurol Neurosurg Psychiatry.* 2008;79(12):1368-74.
470 6. Rao P, and Segal BM. Experimental autoimmune encephalomyelitis. *Methods Mol Med.*
471 2004;102:363-75.
472 7. Segal BM. CNS chemokines, cytokines, and dendritic cells in autoimmune demyelination. *J*
473 *Neurol Sci.* 2005;228(2):210-4.
474 8. Dutta S, and Sengupta P. Men and mice: Relating their ages. *Life Sci.* 2016;152:244-8.
475 9. Lalor SJ, and Segal BM. Th1-mediated experimental autoimmune encephalomyelitis is CXCR3
476 independent. *Eur J Immunol.* 2013;43(11):2866-74.
477 10. Hamann I, Zipp F, and Infante-Duarte C. Therapeutic targeting of chemokine signaling in
478 Multiple Sclerosis. *Journal of the Neurological Sciences.* 2008;274(1-2):31-8.
479 11. Carlson T, Kroenke M, Rao P, Lane TE, and Segal B. The Th17-ELR+ CXC chemokine
480 pathway is essential for the development of central nervous system autoimmune disease. *J Exp*
481 *Med.* 2008;205(4):811-23.

482 12. Kroenke MA, Chensue SW, and Segal BM. EAE mediated by a non-IFN-gamma/non-IL-17
483 pathway. *Eur J Immunol.* 2010;40(8):2340-8.
484 13. Duncker PC, Stoolman JS, Huber AK, and Segal BM. GM-CSF Promotes Chronic Disability in
485 Experimental Autoimmune Encephalomyelitis by Altering the Composition of Central Nervous
486 System-Infiltrating Cells, but Is Dispensable for Disease Induction. *J Immunol.* 2018;200(3):966-
487 73.
488 14. Hammond TR, Dufort C, Dissing-Olesen L, Giera S, Young A, Wysoker A, et al. Single-Cell
489 RNA Sequencing of Microglia throughout the Mouse Lifespan and in the Injured Brain Reveals
490 Complex Cell-State Changes. *Immunity.* 2019;50(1):253-71 e6.
491 15. Mrdjen D, Pavlovic A, Hartmann FJ, Schreiner B, Utz SG, Leung BP, et al. High-Dimensional
492 Single-Cell Mapping of Central Nervous System Immune Cells Reveals Distinct Myeloid
493 Subsets in Health, Aging, and Disease. *Immunity.* 2018;48(2):380-95 e6.
494 16. Wynne AM, Henry CJ, and Godbout JP. Immune and behavioral consequences of microglial
495 reactivity in the aged brain. *Integr Comp Biol.* 2009;49(3):254-66.
496 17. Perry VH, and Holmes C. Microglial priming in neurodegenerative disease. *Nat Rev Neurol.*
497 2014;10(4):217-24.
498 18. von Bernhardi R, Eugenin-von Bernhardi L, and Eugenin J. Microglial cell dysregulation in brain
499 aging and neurodegeneration. *Front Aging Neurosci.* 2015;7:124.
500 19. Batterman KV, Cabrera PE, Moore TL, and Rosene DL. T Cells Actively Infiltrate the White
501 Matter of the Aging Monkey Brain in Relation to Increased Microglial Reactivity and Cognitive
502 Decline. *Front Immunol.* 2021;12:607691.
503 20. Gyoneva S, Hosur R, Gosselin D, Zhang B, Ouyang Z, Cotleur AC, et al. Cx3cr1-deficient
504 microglia exhibit a premature aging transcriptome. *Life Sci Alliance.* 2019;2(6).
505 21. Manich G, Recasens M, Valente T, Almolda B, Gonzalez B, and Castellano B. Role of the
506 CD200-CD200R Axis During Homeostasis and Neuroinflammation. *Neuroscience.*
507 2019;405:118-36.

508 22. Wynne AM, Henry CJ, Huang Y, Cleland A, and Godbout JP. Protracted downregulation of
509 CX3CR1 on microglia of aged mice after lipopolysaccharide challenge. *Brain Behav Immun.*
510 2010;24(7):1190-201.
511 23. Manabe T, Racz I, Schwartz S, Oberle L, Santarelli F, Emmrich JV, et al. Systemic inflammation
512 induced the delayed reduction of excitatory synapses in the CA3 during ageing. *J Neurochem.*
513 2021;159(3):525-42.
514 24. Huber AK, Giles DA, Segal BM, and Irani DN. An emerging role for eotaxins in
515 neurodegenerative disease. *Clin Immunol.* 2018;189:29-33.
516 25. Huber AK, Wang L, Han P, Zhang X, Ekholm S, Srinivasan A, et al. Dysregulation of the IL-
517 23/IL-17 axis and myeloid factors in secondary progressive MS. *Neurology.* 2014;83(17):1500-
518 7.
519 26. Haghikia A, Jorg S, Duscha A, Berg J, Manzel A, Waschbisch A, et al. Dietary Fatty Acids
520 Directly Impact Central Nervous System Autoimmunity via the Small Intestine. *Immunity.*
521 2015;43(4):817-29.
522 27. Rothhammer V, Borucki DM, Tjon EC, Takenaka MC, Chao CC, Ardura-Fabregat A, et al.
523 Microglial control of astrocytes in response to microbial metabolites. *Nature.*
524 2018;557(7707):724-8.
525 28. Duscha A, Gisevius B, Hirschberg S, Yissachar N, Stangl GI, Eilers E, et al. Propionic Acid
526 Shapes the Multiple Sclerosis Disease Course by an Immunomodulatory Mechanism. *Cell.*
527 2020;180(6):1067-80 e16.
528 29. Ruiz-Ruiz S, Sanchez-Carrillo S, Ciordia S, Mena MC, Mendez-Garcia C, Rojo D, et al.
529 Functional microbiome deficits associated with ageing: Chronological age threshold. *Aging Cell.*
530 2020;19(1):e13063.
531 30. Mockus TE, Munie A, Atkinson JR, and Segal BM. Encephalitogenic and Regulatory CD8 T
532 Cells in Multiple Sclerosis and Its Animal Models. *J Immunol.* 2021;206(1):3-10.

533 31. Booss J, Esiri MM, Tourtellotte WW, and Mason DY. Immunohistological analysis of T
534 lymphocyte subsets in the central nervous system in chronic progressive multiple sclerosis. *J*
535 *Neurol Sci.* 1983;62(1-3):219-32.
536 32. Machado-Santos J, Saji E, Troscher AR, Paunovic M, Liblau R, Gabriely G, et al. The
537 compartmentalized inflammatory response in the multiple sclerosis brain is composed of tissue-
538 resident CD8+ T lymphocytes and B cells. *Brain.* 2018;141(7):2066-82.
539 33. Stoolman JS, Duncker PC, Huber AK, Giles DA, Washnock-Schmid JM, Soulika AM, et al. An
540 IFNgamma/CXCL2 regulatory pathway determines lesion localization during EAE. *J*
541 *Neuroinflammation.* 2018;15(1):208.
542 34. Stoolman JS, Duncker PC, Huber AK, and Segal BM. Site-specific chemokine expression
543 regulates central nervous system inflammation and determines clinical phenotype in
544 autoimmune encephalomyelitis. *J Immunol.* 2014;193(2):564-70.
545 35. Balashov KE, Rottman JB, Weiner HL, and Hancock WW. CCR5(+) and CXCR3(+) T cells are
546 increased in multiple sclerosis and their ligands MIP-1alpha and IP-10 are expressed in
547 demyelinating brain lesions. *Proc Natl Acad Sci U S A.* 1999;96(12):6873-8.
548 36. Simpson JE, Newcombe J, Cuzner ML, and Woodroofe MN. Expression of the interferon-
549 gamma-inducible chemokines IP-10 and Mig and their receptor, CXCR3, in multiple sclerosis
550 lesions. *Neuropathol Appl Neurobiol.* 2000;26(2):133-42.
551 37. Fox RJ, Kivisakk P, Fisher E, Tucky B, Lee JC, Rudick RA, et al. Multiple sclerosis: chemokine
552 receptor expression on circulating lymphocytes in correlation with radiographic measures of
553 tissue injury. *Mult Scler.* 2008;14(8):1036-43.
554 38. Marzan DE, Brugger-Verdon V, West BL, Liddelow S, Samanta J, and Salzer JL. Activated
555 microglia drive demyelination via CSF1R signaling. *Glia.* 2021;69(6):1583-604.
556 39. Clark KC, Josephson A, Benusa SD, Hartley RK, Baer M, Thummala S, et al. Compromised
557 axon initial segment integrity in EAE is preceded by microglial reactivity and contact. *Glia.*
558 2016;64(7):1190-209.

559 40. Liddelow SA, Guttenplan KA, Clarke LE, Bennett FC, Bohlen CJ, Schirmer L, et al. Neurotoxic
560 reactive astrocytes are induced by activated microglia. *Nature.* 2017;541(7638):481-7.
561 41. Calderwood SK, Borges TJ, Eguchi T, Lang BJ, Murshid A, Okusha Y, et al. Extracellular Hsp90
562 and protection of neuronal cells through Nrf2. *Biochem Soc Trans.* 2021;49(5):2299-306.
563 42. Yu WW, Cao SN, Zang CX, Wang L, Yang HY, Bao XQ, et al. Heat shock protein 70
564 suppresses neuroinflammation induced by alpha-synuclein in astrocytes. *Mol Cell Neurosci.*
565 2018;86:58-64.
566 43. Chugh D, Iyer CC, Wang X, Bobbili P, Rich MM, and Arnold WD. Neuromuscular junction
567 transmission failure is a late phenotype in aging mice. *Neurobiol Aging.* 2020;86:182-90.
568 44. Sheth KA, Iyer CC, Wier CG, Crum AE, Bratasz A, Kolb SJ, et al. Muscle strength and size are
569 associated with motor unit connectivity in aged mice. *Neurobiol Aging.* 2018;67:128-36.

570

571

572

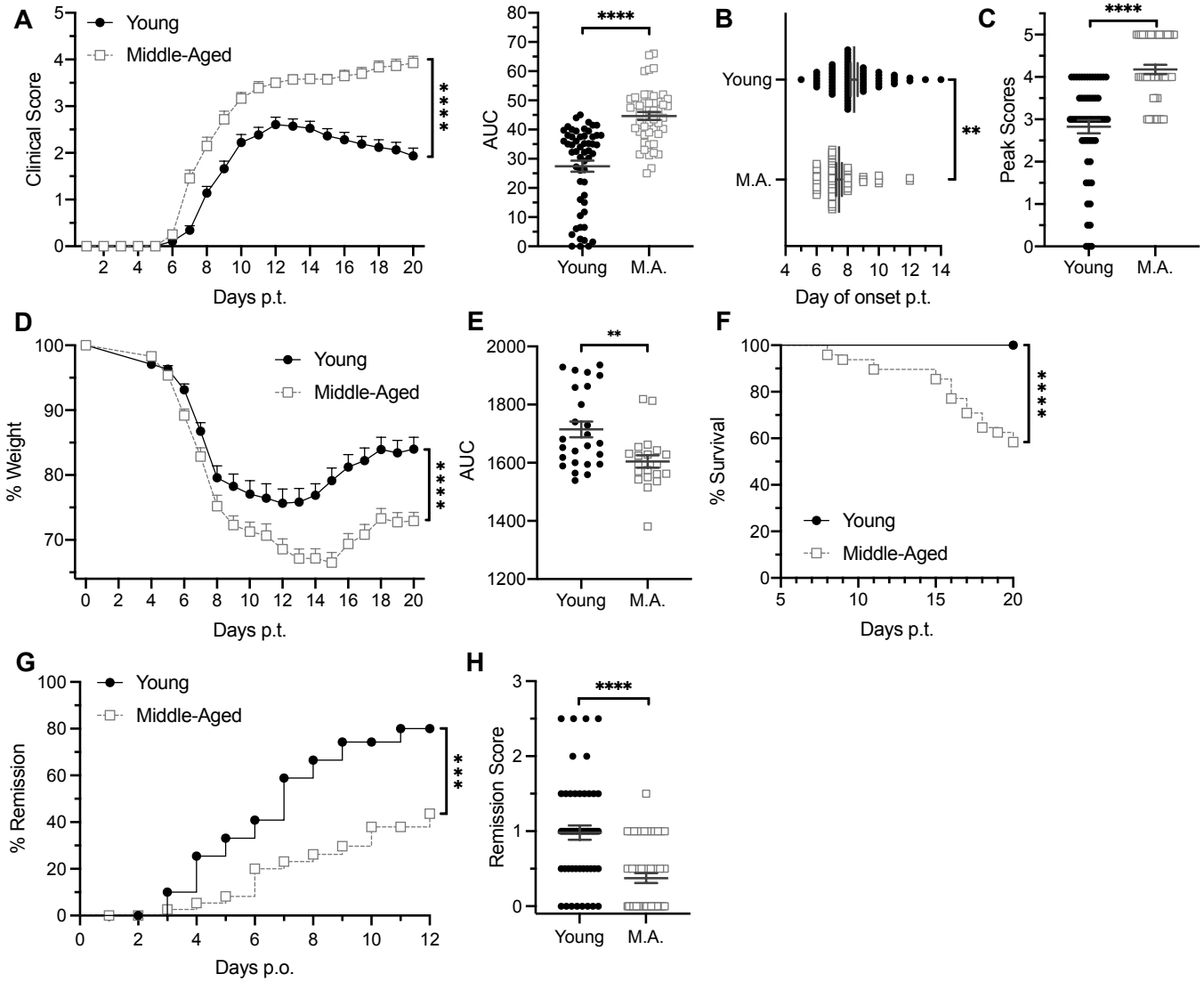

573
574 **Figure 1. Middle-aged mice exhibit an exacerbated, non-remitting course of Th17-mediated adoptive**
575 **transfer EAE.** EAE was induced by the adoptive transfer of myelin-reactive Th17 cells into young or middle-aged
576 mice. (**A-C**) Young (n=70) and middle-aged (n=62) adoptive transfer recipients were scored daily for severity of
577 neurological deficits by an examiner blinded to the identity of experimental groups. Data were pooled from 4
578 independent experiments. (**A**) Mean clinical scores of young and middle-aged hosts over time (left panel). The
579 area under the curve (AUC) was measured for individual mice in each group (right panel). (**B**) Day of disease
580 onset post-transfer and (**C**) peak clinical disease scores of individual mice. (**D**) Young (n=40) and middle aged
581 (n=36) recipients were weighed on a daily basis. Data were pooled from 3 independent experiments. The % of
582 baseline weight over time, averaged across young and middle-aged recipients (left panel). The area under the
583 curve (AUC) was measured for individual mice in each group (right panel). (**E**) Percent survival over the disease
584 course. (**F**) Percent of mice undergoing remission on each day post clinical onset (left panel). (**H**) Difference
585 between clinical score at peak disease minus score at day 20 post- cell transfer for each mouse. Each symbol
586 in **B** and **C**, and the right panels of **A**, **D**, and **F**, represents data generated from a single mouse. Statistical
587 significance was determined using unpaired 2-tailed Student's *t* test. Curves in the left panels of **A** and **D** were
588 compared using a mixed effects model. Curves in **F** and **G** were compared using the Log rank test. Error bars
589 indicate mean ± SEM. *p <0.05, **p <0.01, ***p <0.001, ****p <0.0001.

590

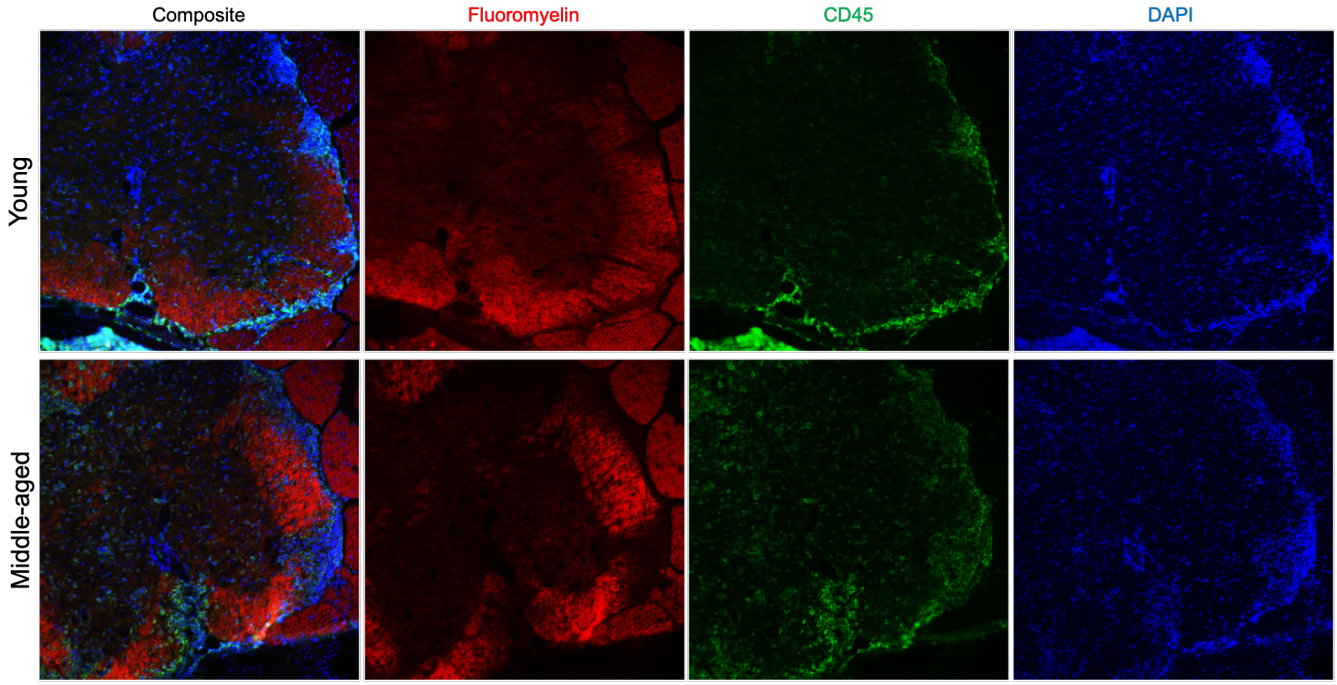

591

592 **Figure 2. Spinal cord demyelination and inflammatory infiltration are exacerbated in middle-aged**
593 **recipients.** Representative spinal cord sections of young (upper panels) and middle-aged (lower panels) adoptive
594 transfer recipients of encephalitogenic Th17 cells. Sections were stained for myelin (Fluoromyelin; red), CD45
595 (green), and DAPI (blue). All images were acquired at 20x magnification.

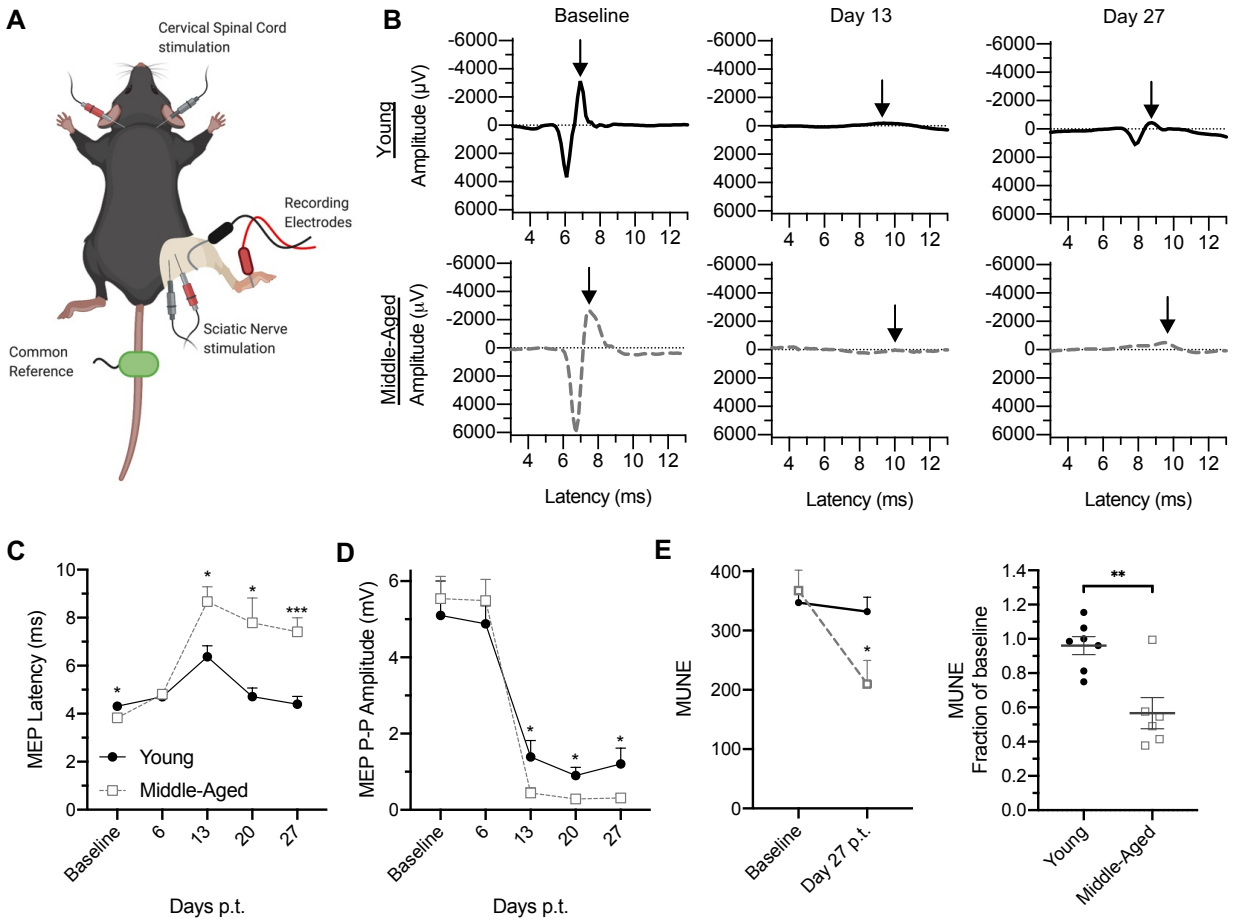

Figure 3. Electrophysiological studies indicate increased demyelination and neuronal/axonal drop out in the spinal cords of middle-aged mice with EAE.
(**A-E**) EAE was induced in young adult (n=10) and middle-aged (n=10) mice by the adoptive transfer of encephalitogenic MOG-specific CD4+ T cells. Mice were anaesthetized for electrographic recordings. (**A**) Depiction of electrode placement. (**B**) Representative cervical motor-evoked potentials recorded from the right gastrocnemius following cervical spinal cord stimulation at baseline, day 13, and day 27 post-cell transfer. Arrows indicate negative peaks of the cervical motor-evoked potentials. (**C, D**) Electrographic measurements were obtained at baseline and then on a weekly basis. Measurements of motor-evoked potential latency (**C**), and peak-to-peak (P-P) amplitude (**D**) were averaged across each group. (**E**) Motor unit number estimation (MUNE) was calculated at baseline and on day 27 post transfer. Mean values for each group are shown (left panel). The ratio of MUNE at day 27 post-cell transfer over baseline is shown for individual mice (right panel). Statistical significance determined by unpaired 2-tailed Student's *t* test. *p <0.05, **p <0.01, ***p <0.001. Error bars indicate mean ± SEM.

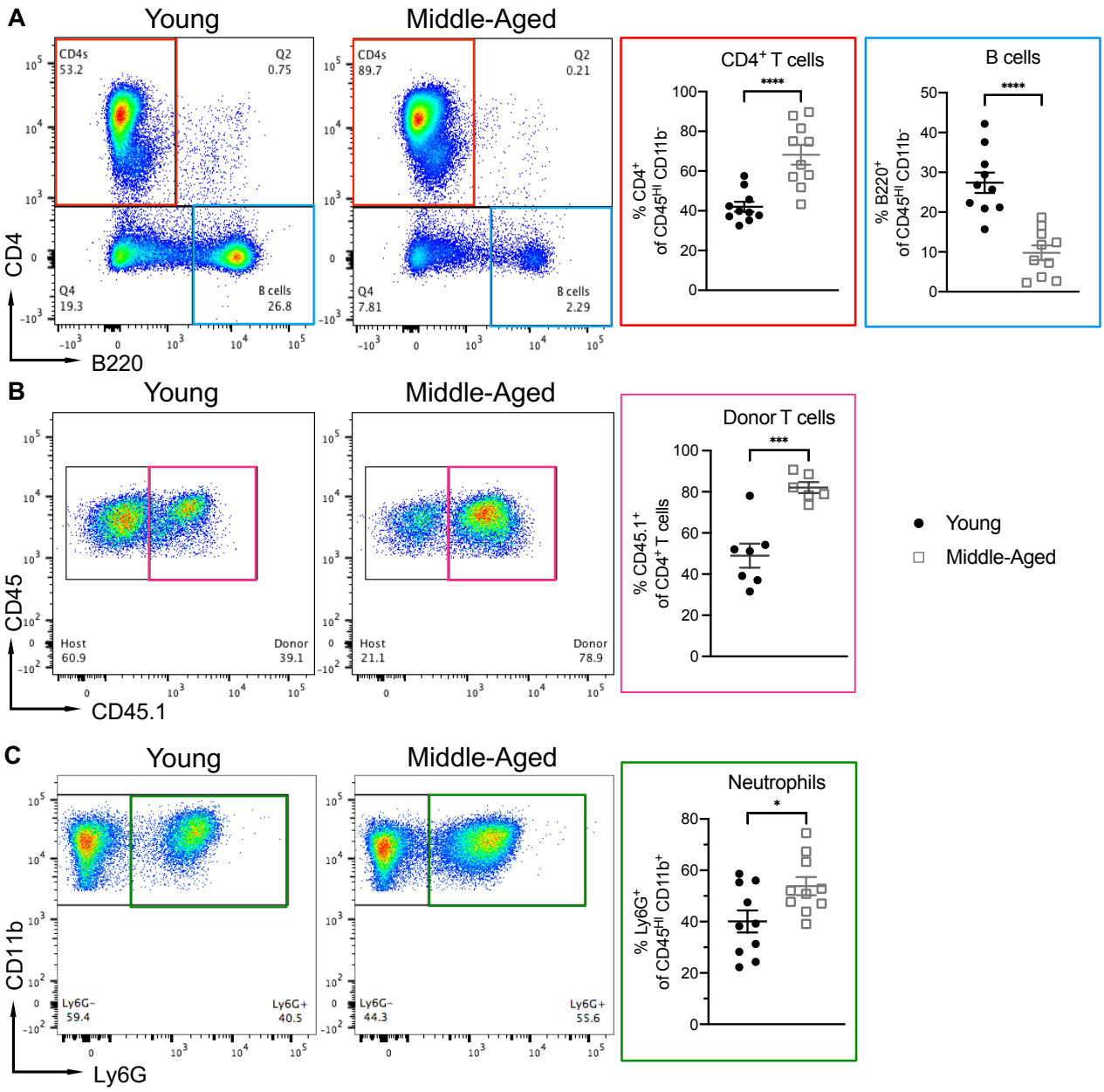

Figure 4. The composition of CNS-infiltrating immune cells differs between middle-aged and young adult mice with EAE. (**A-C**) Mononuclear cells were isolated from the spinal cords of young adult and middle-aged mice on day 10 post-transfer of encephalitogenic CD45.1$^+$ CD4$^+$ T cells for flow cytometric analysis, gating on all CD45$^+$ cells. Representative dot plots, as well as the frequencies of CD4$^+$ T cells and B cells (**A**), CD45.1$^+$ donor T cells (**B**), and neutrophils (**C**), are shown. Each symbol represents an individual mouse. Data were pooled from 3 independent experiments with a total of 7-10 mice per group. Statistical significance was determined using the unpaired 2-tailed Student's *t* test. *p <0.05, ***p <0.001, ****p <0.0001. Error bars indicate mean ± SEM.

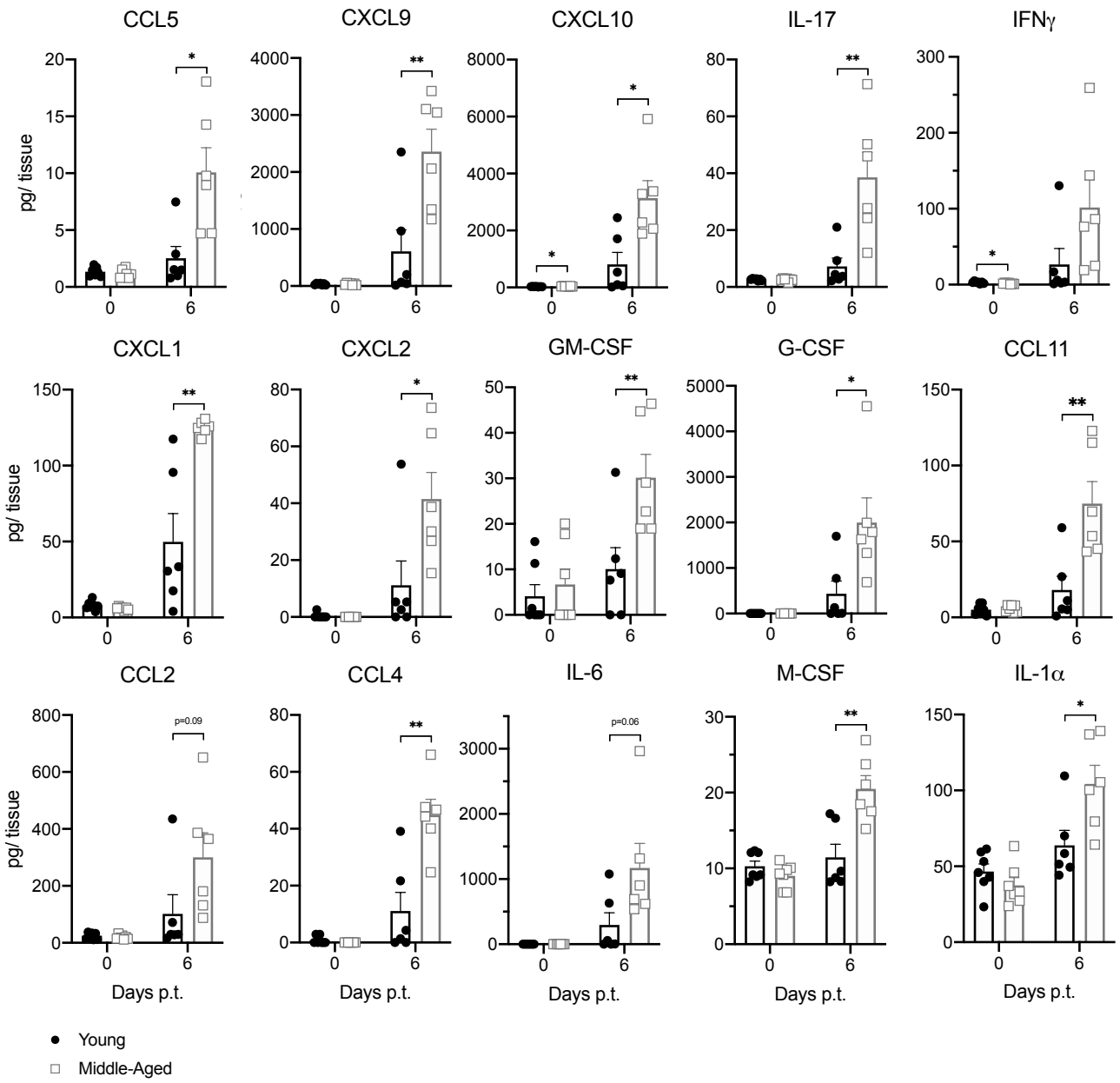

Figure 5. Pro-inflammatory proteins and elevated in the spinal cords of middle-aged mice with adoptive transfer EAE. Spinal cord homogenates were obtained from young (closed circles) and middle-aged (open squares) naïve mice (left bars) or adoptive transfer recipients on day 6 post-transfer (right bars). A panel of pro-inflammatory factors were measured using the Luminex bead-based multiplex platform. Data were pooled from 2-4 independent experiments with a total of 7-13 mice/group. Each symbol represents a single mouse. Statistical significance was determined using the unpaired 2-tailed Student's *t* test. *p <0.05, ***p <0.001, ****p <0.0001. Error bars indicate mean ± SEM.

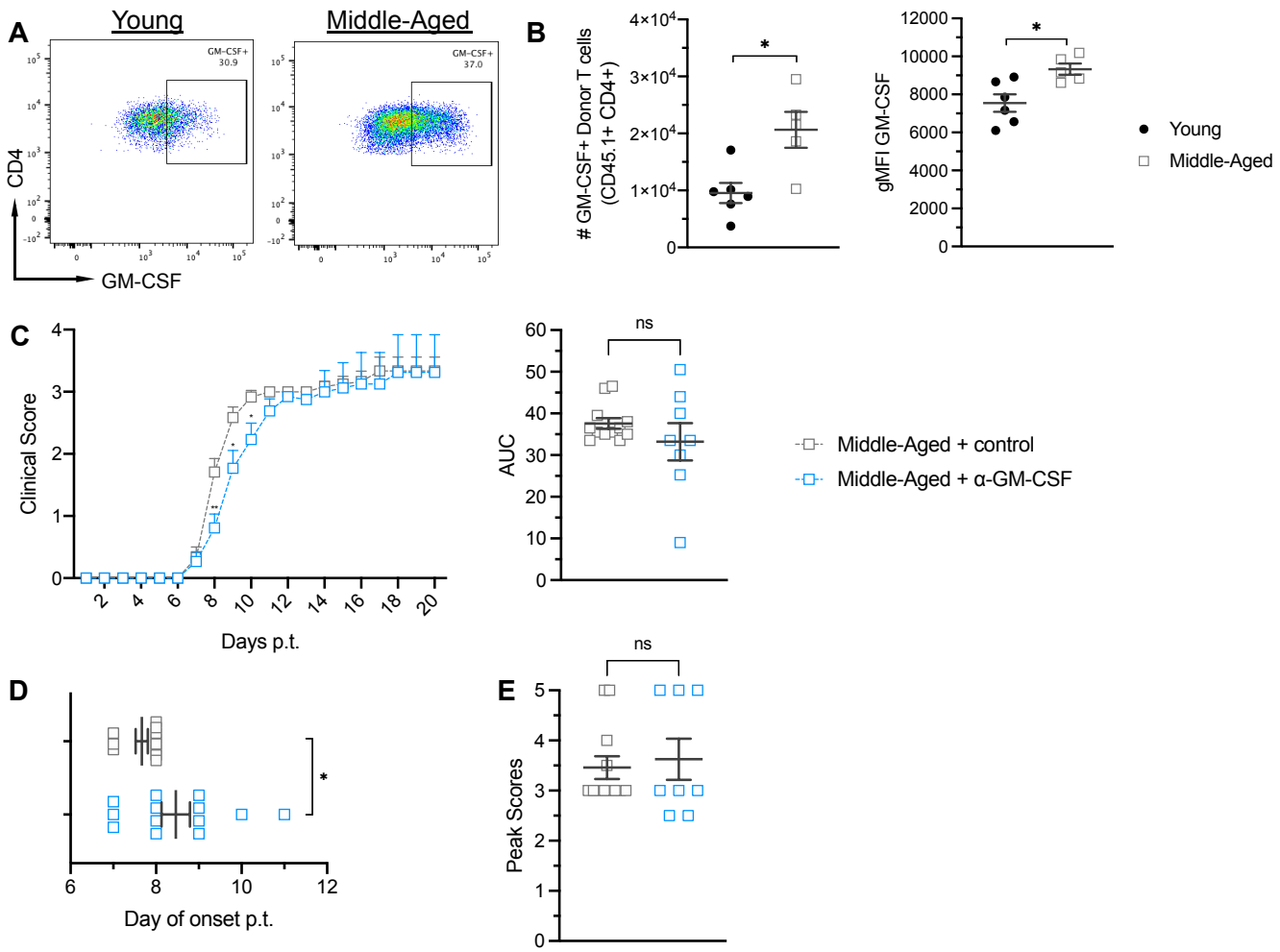

Figure 6. GM-CSF promotes exacerbated EAE in middle-aged mice early, but not late, in the clinical course. (**A, B**) CNS mononuclear cells were harvested from the spinal cords of young adult and middle-aged mice on day 10 post-T cell transfer for analysis by flow cytometry. (**A**) Representative dot plots showing intracellular GM-CSF expression, gating on CD45.1$^+$ donor CD4$^+$ T cells. (**B**) Total number of GM-CSF$^+$ donor T cells (left panel), and geometric mean fluorescent intensity (gMFI) of GM-CSF in donor T cells (right panel), isolated from the spinal cords of individual mice. Data were pooled from 2 independent experiments with 5-6 mice/group. (**C-E**) Middle-aged mice were injected i.p. with anti-GM-CSF neutralizing antibody or control antibody every other day from the time of encephalitogenic T cell transfer onward (n= 14 mice/group; pooled from 2 independent experiments). Mice were scored for severity of neurological deficits on a daily basis by raters blinded to the identity of the experimental groups. (**C**) Mean clinical scores of mice in each group over time (left panel). Area under the curves (AUC) of individual mice (right panel). (**D**) Day of clinical disease onset post-transfer and (**E**) peak clinical disease scores of individual mice. Statistical significance was determined using the unpaired 2-tailed Student's *t* test. *p <0.05 or as indicated. Error bars indicate mean ± SEM.

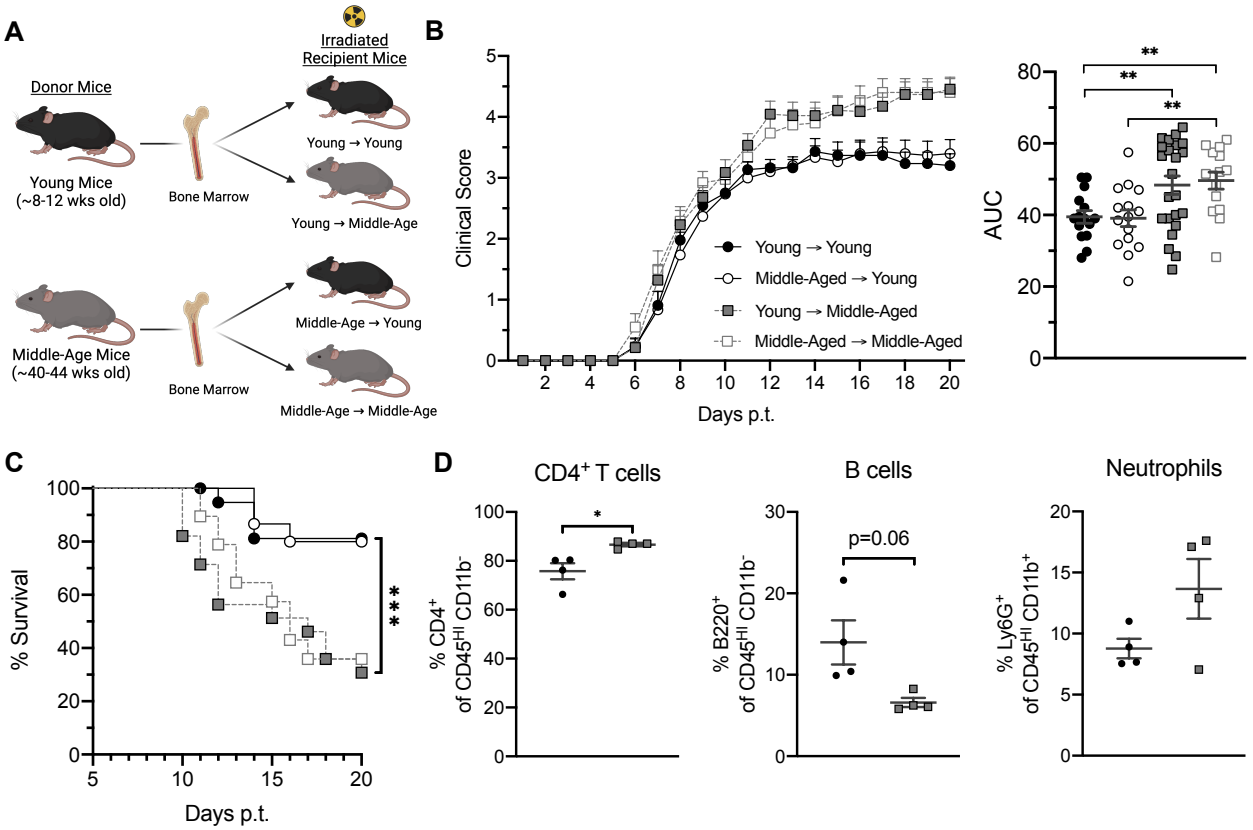

Figure 7. Radio-resistant, non-hematopoietic cells drive exacerbated EAE in middle-aged mice. (**A-D**) Reciprocal bone marrow chimeric mice were constructed with young adult or middle-aged donors and hosts. Following reconstitution, all chimeric mice were injected i.p. with 3 x 10^6 MOG-primed $CD4^+$ Th17 cells. Mice were scored for severity of neurological deficits on a daily basis by raters blinded to the identity of the experimental groups. (**A**) Schematic depicting the construction of reciprocal bone marrow chimeras. (**B**) Mean clinical scores over time (left panel) and area under the curves (AUC) of individual mice (right panel). (**C**) Percent of surviving mice in each group over time. (**D**) Frequencies of $CD4^+$ T cells, B cells, and neutrophils among $CD45^+$ spinal cord mononuclear cells harvested from individual mice on day 10 post-transfer. Data in (**B**) and (**C**) were pooled from 3 independent experiments with a total of 15-28 mice per group. Each symbol in B, right panel, and in D represent an individual mouse, Data in (**D**) are representative experiment of 3 independent experiments (n=4 mice/group). Statistical significance was determined using the unpaired 2-tailed Student's *t* test. Curves in **C** were compared using the Log rank test. *p <0.05, **p <0.01, ***p <0.001 or as indicated. Error bars indicate mean ± SEM.

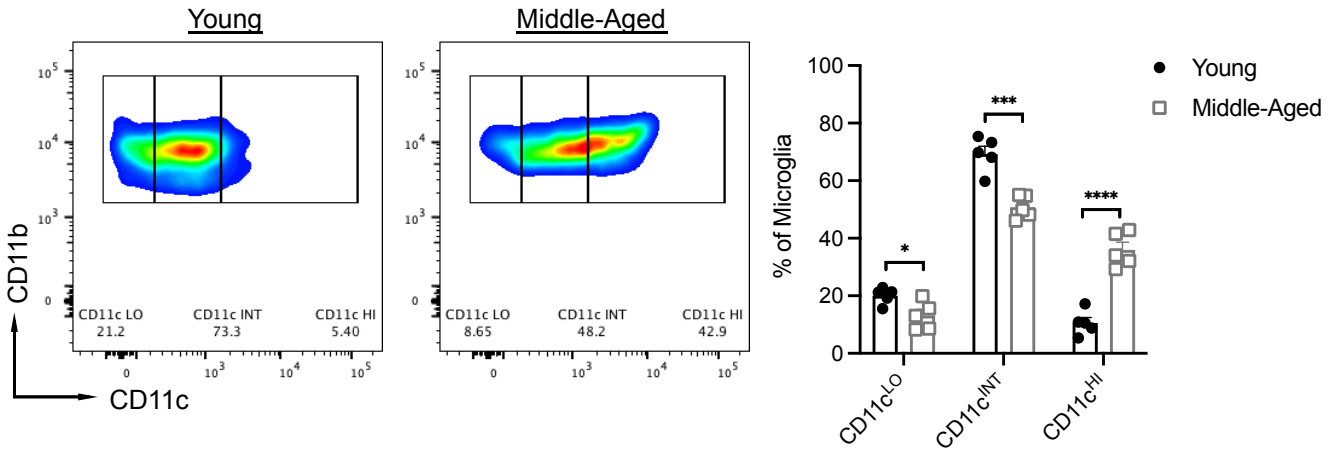

Figure 8. Subpopulations of microglia in middle-aged mice up-regulate CD11c. Mononuclear cells were harvested from the spinal cords of naïve young adult and middle-aged mice. Representative dot plots (left and middle panel), and frequencies of $CD11c^{lo}$, $CD11c^{int}$ and $CD11c^{hi}$ cells among $CD45^{int}$CD11b+ microglia (right panel), are shown. Each symbol in the right panel represents an individual mouse. Data were pooled from 2 independent experiments with n=5 mice/group. Statistical significance was determined using the unpaired 2-tailed Student's *t* test. *p <0.05, ***p <0.001, ****p <0.0001. Error bars indicate mean ± SEM.

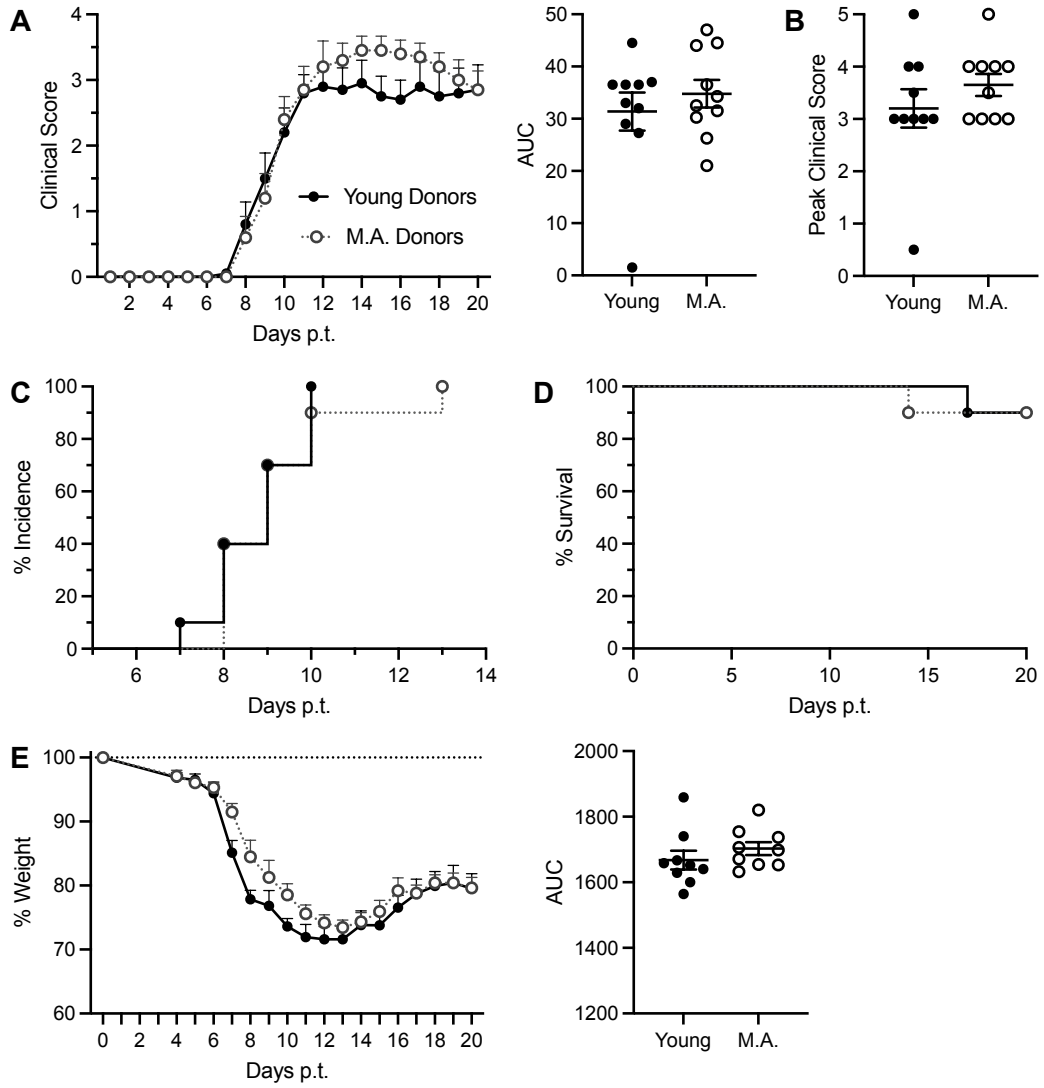

662

663 **Supplementary Figure 1. Age of MOG-primed donors does not impact disease severity in CD4$^+$ T cell**
664 **recipient mice.** A) Clinical score curves of mean disability in recipient mice receiving young or middle-aged donor
665 CD4$^+$ T cells (left) and area under the curve (AUC) analysis of clinical score curves for individual mice (right). B)
666 Peak clinical disease score for individual mice and curves indicating the percentage of mice (C) demonstrating
667 clinical disease onset and (D) survival throughout the duration of the EAE time-course are shown. E) Percent of
668 baseline weight for young and middle-aged mice throughout EAE time-course (left) and AUC analysis of percent
669 weight curves for individual mice (right). Data represent pooled mice (n=10 mice/group) from one independent
670 experiment.

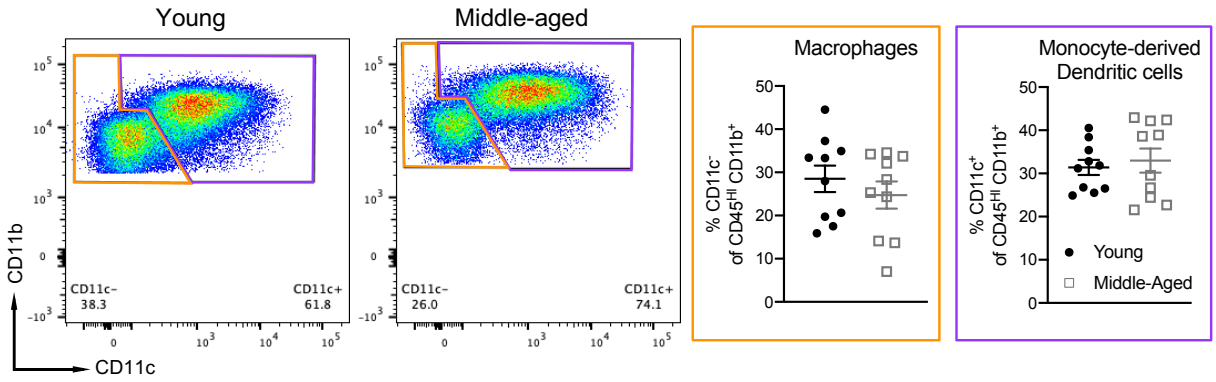

Supplementary Figure 2. Frequencies of monocyte-derived dendritic cells and macrophages did not differ between young and middle-aged mice during EAE. CNS inflammatory cells were harvested from the spinal cords of young and middle-aged mice at day 10 post-transfer. Representative plots and frequencies of macrophages ($CD45^+$ $CD11b^+$ $Ly6G^-$ $CD11c^-$) and monocyte-derived dendritic cells ($CD45^+$ $CD11b^+$ $Ly6G^-$ $CD11c^-$) for individual mice. Data consists of pooled mice (n=10 mice/group) from 3 independent experiments. Each symbol represents a data point generated from a single mouse with statistical significance determined by unpaired 2-tailed Student's *t* test.